Advanced Composite Materials
Publication details, including instructions for authors and subscription information:
http://www.tandfonline.com/loi/tacm20

Experimental Characterization of Dynamic Tensile Strength in Unidirectional Carbon/Epoxy Composites

Norihiko Taniguchi [a], Tsuyoshi Nishiwaki [b] & Hiroyuki Kawada [c]
[a] Research Institute of Sports Science, ASICS Corporation, 6-2-1 Takatsukadai, Nishi-ku, Kobe 65a-2271, Japan
[b] Department of Mechanical Engineering, Waseda University, Tokyo, Japan
[c] Department of Mechanical Engineering, Waseda University, Tokyo, Japan
Version of record first published: 02 Apr 2012.

///VSP///

Advanced Composite Materials 17 (2008) 139–156

ADVANCED COMPOSITE MATERIALS
www.brill.nl/acm

Experimental Characterization of Dynamic Tensile Strength in Unidirectional Carbon/Epoxy Composites

Norihiko Taniguchi [a,*], **Tsuyoshi Nishiwaki** [b] **and Hiroyuki Kawada** [b]

[a] Research Institute of Sports Science, ASICS Corporation, 6-2-1 Takatsukadai, Nishi-ku, Kobe 65a-2271, Japan

[b] Department of Mechanical Engineering, Waseda University, Tokyo, Japan

Received 26 March 2007; accepted 19 September 2007

Abstract

This study aims to characterize the dynamic tensile strength of unidirectional carbon/epoxy composites. Two different carbon/epoxy composite systems, the unidirectional T700S/2500 and TR50S/modified epoxy, are tested at the static condition and the strain rate of 100 s^{-1}. A high-strain-rate test was performed using a tension-type split Hopkinson bar technique with a specific fixture for specimen. The experimental results demonstrated that both tensile strength increase with strain rate, while the fracture behaviors are quite different. By the use of the rosette analysis and the strain transformation equations, the strain rate effects of material principal directions on tensile strength are investigated. It is experimentally found that the shear strain rate produces the more significant contribution to strain rate effect on dynamic tensile strength. An empirical failure criterion for characterizing the dynamic tensile strength was proposed based on the Hashin's failure criterion. Although the proposed criterion is just the empirical formula, it is in better agreement with the experimental data and quite simple.

Keywords

Impact behavior, tensile strength, failure criterion, carbon/epoxy composite, split Hopkinson bar

1. Introduction

Carbon/epoxy composites have been widely used not only in traditional aerospace structures, but also in sports gear [1], which are subjected to dynamic loads. The tensile strength of composite materials is one of the most important material properties in the design process. It has been recognized that carbon/epoxy composite exhibits a rate dependency [2, 3]. Therefore, it is important to obtain the accurate tensile strength under the high strain rate condition.

* To whom correspondence should be addressed. E-mail: nori@tiger4.sp.asics.co.jp

DOI:10.1163/156855108X314779

There are a number of researches who have investigated the dynamic tensile behavior of composite materials [4, 5]. Thiruppukuzhi and Sun [6] characterized the rate-dependent tensile behavior of the unidirectional S2-glass/8553 and the woven E-glass/7781 composites. Although the model prediction is shown to be adequate for capturing the strain rate effect on tensile strength, the maximum strain rate, i.e. 1.0 s^{-1}, is not sufficient as a high strain rate condition. Harding and Welsh [7] conducted an impact tensile test of unidirectional carbon/epoxy composite with a modification of split Hopkinson bar (SHB) method. It has been shown that the tensile strength and failure mode in the fiber direction were independent of strain rate. Staab and Gilat [8] investigated the strain rate dependence of tensile strength in the case of angle-ply glass/epoxy laminates. They concluded that the fibers had a greater influence on strain rate effect than the matrix. The authors [9] proposed the tension-type SHB apparatus with a specific fixture for impact tensile specimen. Their experimental results show that the shear and transverse tensile strength increase with the strain rate, while the tensile strength in the longitudinal direction is independent of the strain rate. Further, the strain rate dependence of the shear strength is much stronger than that of the transverse strength.

This study aims to characterize the dynamic tensile strength of unidirectional carbon/epoxy composites, whose dominant failure mode is shear and transverse fracture. The two different material systems, whose interfacial and matrix properties are different, are tested at the static condition and the strain rate of 100 s^{-1}. The strain rate effect on tensile strength of carbon/epoxy composites is experimentally examined. In order to investigate the difference of fracture behavior, the fracture surface observation is also performed. Further, the strain rate effect of the material principal directions on tensile strength is individually discussed. Finally, the empirical rate-dependent failure criterion, which is based on Hashin's failure criterion [10], is proposed.

2. Static Test

The 0, 10, 15, 30, 45, 60, 75 and 90° coupon specimens were fabricated from unidirectional composite prepregs. The two different carbon/epoxy composite systems — the unidirectional T700S/2500 (Toray Industries, Inc.) and TR50S/modified epoxy (Mitsubishi Rayon Co. Ltd.) — were tested. The end tabs were cut from glass/epoxy composite panels and then bonded on the specimens. The specimen geometry is shown in Fig. 1.

Static tensile test was carried out using the universal testing machine, Instron 4204, with a constant strain rate of 1.04×10^{-4} s^{-1}. Longitudinal strain was measured from the strain gauges (KFG-3-120-C1-11, Kyowa Electronic Instruments Co. Ltd.) glued at the center of coupon specimens. The shear strength were calculated from the 10° off-axis specimens by the transformation equations of stress as

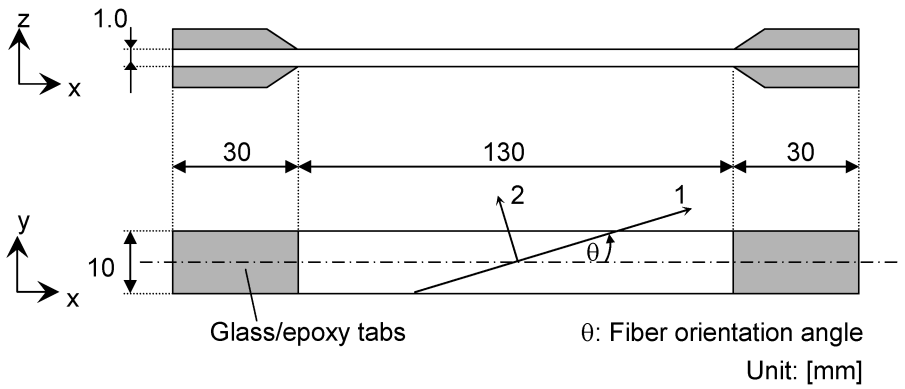

Figure 1. Specimen geometry and position of strain gauge for static test.

follows [11]:

$$\begin{aligned} \sigma_1 &= \sigma_x \cos^2\theta, \\ \sigma_2 &= \sigma_x \sin^2\theta, \\ \tau_{12} &= -\sigma_x \sin\theta\cos\theta, \end{aligned} \tag{1}$$

where the stresses σ_{ij} refer to the principal material direction and σ_x is the applied stress. The parameter σ denotes the angle between loading and fiber direction.

Figure 2(a) and 2(b) shows typical examples of stress–strain curve for all specimens. The measured tensile strength in material principal directions is also summarized in Table 1. No difference can be confirmed in the longitudinal strength in the two composites. On the other hand, it is shown that the shear and transverse strength of TR50S/modified epoxy (TR5S-m) are higher than that of T700S/2500 (T7S-2). These experimental results imply that the interfacial or matrix properties of TR5S-m, such as the strength and toughness, are higher than those of T7S-2.

3. Dynamic Test

3.1. Off-axis Specimen With an Oblique Tab

Two different carbon/epoxy composite systems described in the previous section were tested. It has been experimentally demonstrated that the tensile strength in the longitudinal direction is independent of the strain rate [9]. Hence, the 10, 15, 30, 45, 60, 75 and 90° coupon specimens were employed in the dynamic test. Figure 3 shows the geometry of the off-axis specimen. In order to minimize the extension-shear coupling effect, the oblique tab proposed by Sun and Chung [12] was employed, in which the oblique angle ϕ is expressed as follows,

$$\cot\phi = -\frac{\bar{S}_{16}}{\bar{S}_{11}}, \tag{2}$$

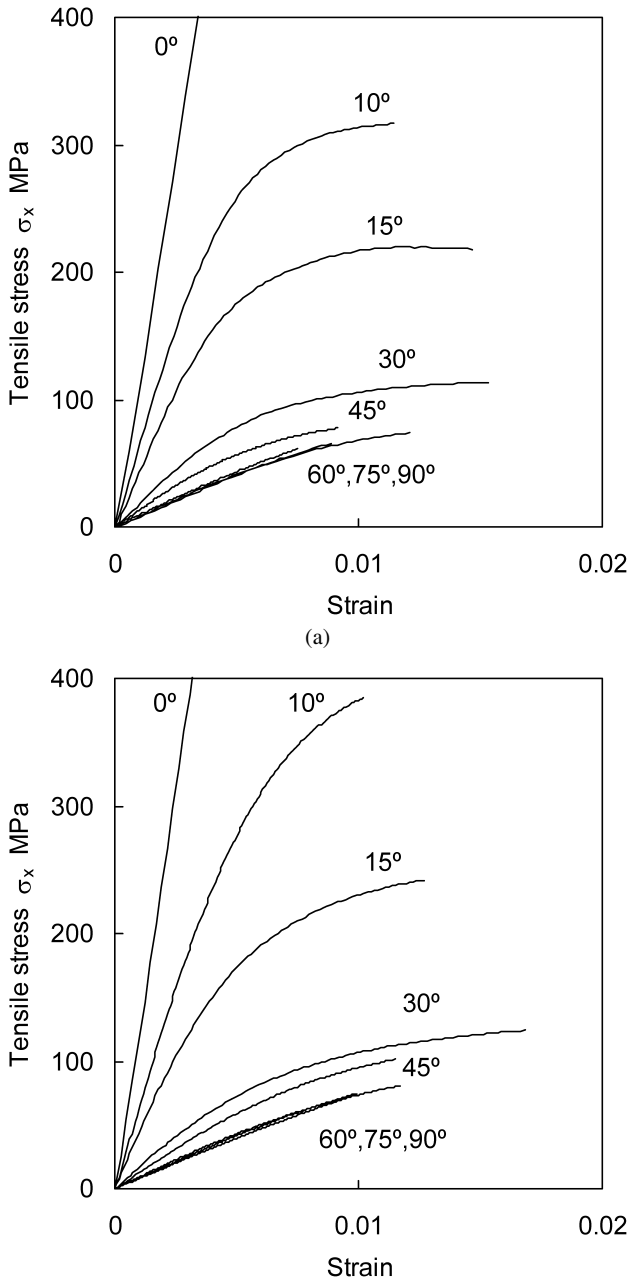

Figure 2. (a) Stress–strain curves for the 0, 10, 15, 30, 45, 60, 75 and 90° specimens under the static condition (T700S/2500); (b) stress–strain curves for the 0, 10, 15, 30, 45, 60, 75 and 90° specimens under the static condition (TR50S/modified epoxy).

Table 1.
Tensile strength for each material under static loading condition

Material principal direction	T700S/2500	TR50S/modified epoxy
Longitudinal X (GPa)	2.36	2.31
Transverse Y (MPa)	63.1	72.6
Shear S (MPa)	56.5	65.4

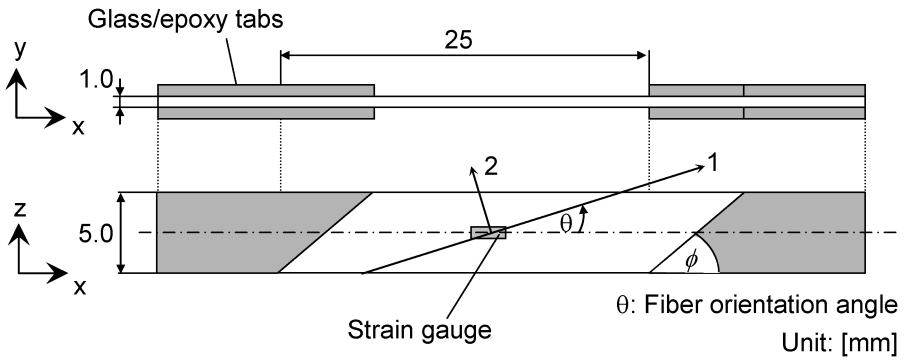

Figure 3. Geometry of off-axis specimen with oblique tab.

where $\bar{S}_{ij}$ is the compliance coefficients with respect to the x–y coordinate system. The employed oblique angle is shown in Fig. 4 as a function of fiber orientation angle. It is noted that the conventional tabs are employed for the 90° specimens.

3.2. Experimental Method

A high-strain-rate test was performed using a tension-type SHB technique. Figure 5(a) and 5(b) shows schematic drawings of the experimental system employed in this study. The system consists of an input bar with a flange, an output bar, and a cylindrical striker. The input and output bars made of steel have a diameter of 16 mm, and a length of 2000 and 1500 mm, respectively. A cylindrical striker made of steel has an outer diameter of 22.8 mm, and an inner diameter of 16.2 mm. In order to control the fluctuating behavior during tensile loading, a piece of brass (outer and inner diameter: 22.0 and 16.2 mm, thickness: 1.0–5.0 mm) is sandwiched between a cylindrical striker and an input bar. Hence, a ramped incident wave is induced by the plastic deformation of brass [13]. The data obtained from the SHB method comprise the strain histories of the input and output bars. In this study, the strain histories are recorded from the strain gauges with a gauge length of 1.0 mm at a sampling rate of 1.0 MHz *via* a DC amplifier (upper frequency limit: 100 kHz). General-purpose foil (KFG-1-350-C1-11, Kyowa Electronic Instruments Co. Ltd.) and semiconductor strain gauges (KSP-1-350-E4, Kyowa Electronic Instruments Co. Ltd.) are glued onto the input and output bars, respectively. A special fixture for the impact tensile specimen is employed in this study [9]. The fixture design is

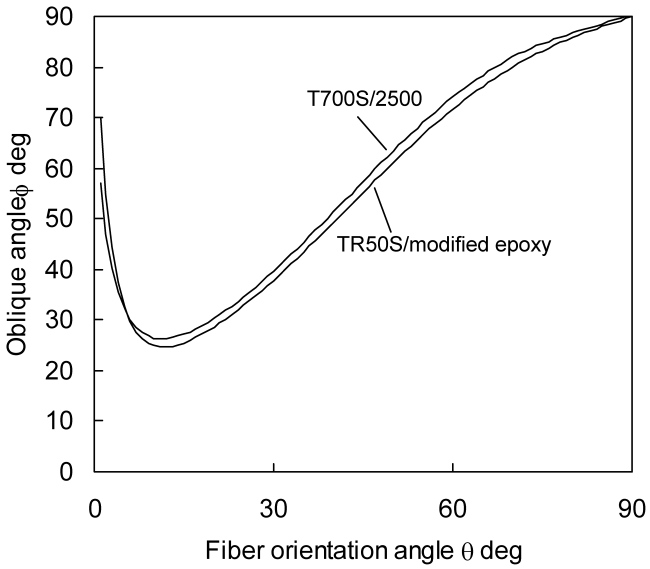

Figure 4. Employed oblique angle for T700S/2500 and TR50S/modified epoxy off-axis specimen at strain rate of 100 s^{-1}.

schematically illustrated in Fig. 5(b). The bar end has a tapered thread and a slot that is diametrically parallel to the region where the specimen is inserted. A saw-toothed slotted area is machined with precision. A compression ring with a thread, which compensates for the area loss caused by the slot, is mounted at the bar ends to fix the specimen. It was found that this fixing technique can transmit tensile loads of up to 3000 N at the present.

In the SHB system, the stress can be calculated by the one-dimensional wave propagation theory [14], that is,

$$\sigma = \frac{AE(\varepsilon_{\mathrm{i}} + \varepsilon_{\mathrm{r}})}{A_{\mathrm{s}}} = \frac{AE(\varepsilon_{\mathrm{t}})}{A_{\mathrm{s}}}, \tag{3}$$

where $\varepsilon_{\mathrm{i}}, \varepsilon_{\mathrm{r}}$ and ε_{t} denote the incident, reflected and transmitted strain waves, respectively. Further, E denotes the Young's modulus of the bar; A, the cross-sectional area of the bar; A_{s}, the cross-sectional area of the specimen.

Figure 6 shows a typical example of strain gauge output for a 15° specimen. An important assumption in equation (3) is that the wave propagation effects within the specimen are negligible. In other words, the load P_{i} between the input bar and specimen may be equivalent to the load P_{o} between the output bar and specimen (it follows that $\varepsilon_{\mathrm{i}} + \varepsilon_{\mathrm{r}} = \varepsilon_{\mathrm{t}}$). Figure 7 shows the comparison of load P_{i} and P_{o} for 15° specimens. The experimental result shows that the values for the load P_{i} almost agree with the load P_{o}, except for the initial stage. Hence, the equation (3) is applicable in this study; the tensile strength can be determined from the transmitted strain wave. Also, strain and strain rate of the specimen are directly measured from the strain gauge glued onto the specimen [9, 15].

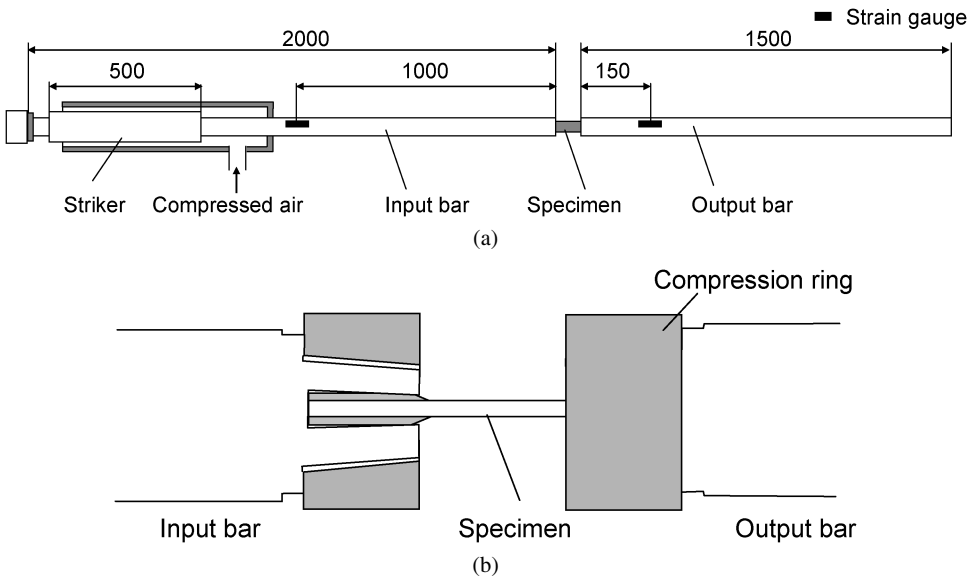

Figure 5. (a) Tension-type SHB apparatus constructed in this study; (b) a schematic drawing of fixture design in this study.

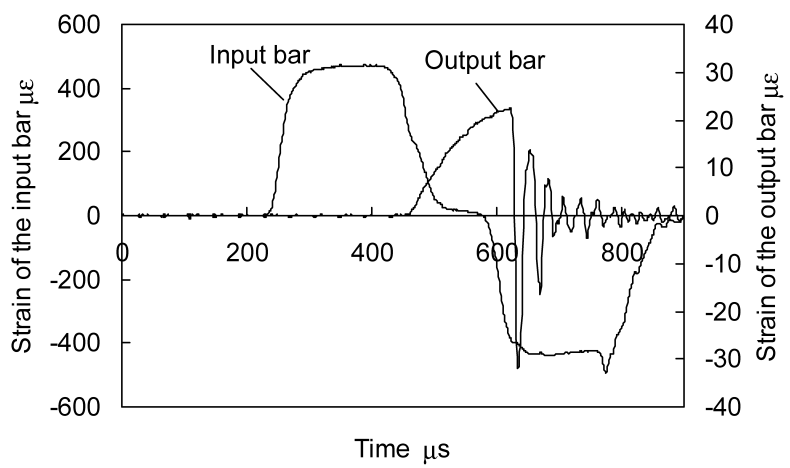

Figure 6. Strain gauge outputs from the input and output bars for the 15° specimen.

3.3. Stress–Strain Curves

In off-axis specimens, it is important to achieve a state of uniform stress (uniform strain) during dynamic tensile loading. To obtain the strain distribution, three strain gauges were mounted on 15° off-axis specimen, where the extension-shear coupling effect is the most prominent. The strain distribution with rectangular tab is also measured for comparison. Figure 8(a) and 8(b) shows the comparison of strain between the conventional and oblique tabs at strain rate of $\dot{\varepsilon} = 100\ \mathrm{s}^{-1}$. The strain gauge

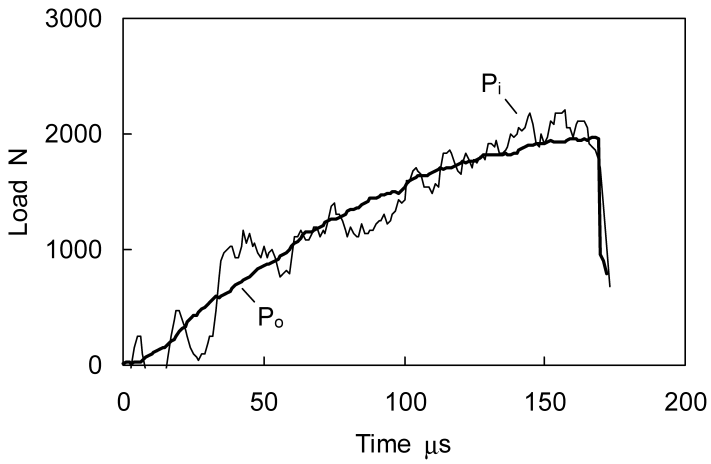

Figure 7. Comparison of load histories of 15° specimen at each face of the bars.

positions and the photograph of fractured specimens are also shown. In Fig. 8(a), a large stress concentration can be observed at gauge position 3, which leads to the premature failure at the tabbed area. On the other hand, the strain distribution is almost uniform when oblique tabs are employed (see Fig. 8(b)). Further, the failure position was mainly in the gauge section of the specimen. These experimental results indicate that the oblique tab is superior to the conventional tabs for evaluating the dynamic tensile strength of off-axis specimen.

Typical examples of stress–strain curves for the 10, 15, 30, 45, 60, 75 and 90° specimens, whose strain rates are $\dot{\varepsilon} = 100\ \mathrm{s}^{-1}$ are shown in Fig. 9(a) and 9(b) for T7S-2 and TR5S-m, respectively. Compared with the Fig. 2(a) and 2(b), it can be said with fair certainty that the dynamic tensile strength of both materials is higher than those of static test for all fiber orientation angles.

4. Discussion

4.1. Strain Rate Effect on Tensile Strength

Tensile strengths of 10, 15, 30, 45, 60, 75 and 90° specimens tested at two strain rates are obtained. Figure 10(a) and 10(b) shows the comparison of tensile strength between static and strain rate of $\dot{\varepsilon} = 100\ \mathrm{s}^{-1}$ for T7S-2 and TR5S-m, respectively. The summary of tensile strength is listed in Table 2. In both materials, it is obvious that the higher fiber-orientated specimens, such as 10, 15 and 30° specimens, produce the more significant contribution to the strain rate dependency of tensile strength. It is experimentally possible to divide the strain rate in the loading direction $\dot{\varepsilon}$ into each principal material direction, that is $\dot{\varepsilon}_1, \dot{\varepsilon}_2$ and $\dot{\gamma}_{12}$. In order to investigate the effect of strain rate in the principal material directions on tensile strength, the triaxial strain gauge (KGF-1-120-D17-11, Kyowa Electronic Instruments Co. Ltd.) was glued onto each specimen. Typical examples of strain gauge

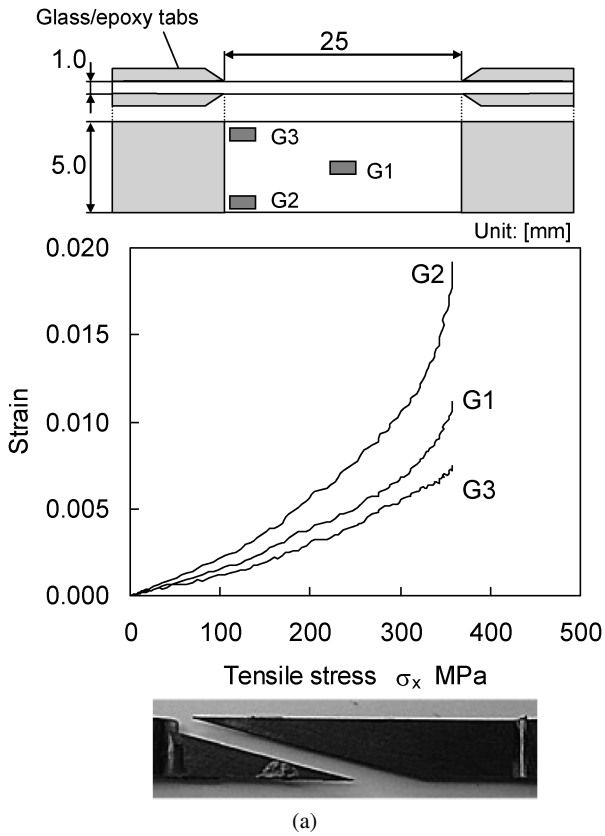

(a)

Figure 8. (a) Strain distributions and fracture position of 15° specimen with rectangular tabs; (b) strain distributions and fracture position of 15° specimen with oblique tabs.

outputs measured from triaxial gauge are shown in Fig. 11. By the application of the rosette analysis and the strain transformation equations expressed as follows, the strain rate in the material principal directions can be obtained:

$$\begin{aligned}
\dot{\varepsilon}_1 &= \dot{\varepsilon}_x \cos^2\theta + \dot{\varepsilon}_y \sin^2\theta + \dot{\gamma}_{xy} \sin\theta\cos\theta, \\
\dot{\varepsilon}_2 &= \dot{\varepsilon}_x \sin^2\theta + \dot{\varepsilon}_y \cos^2\theta - \dot{\gamma}_{xy} \sin\theta\cos\theta, \\
\frac{\dot{\gamma}_{12}}{2} &= -\dot{\varepsilon}_x \sin\theta\cos\theta + \dot{\varepsilon}_y \sin\theta\cos\theta + \frac{\dot{\gamma}_{xy}}{2}(\cos^2\theta - \sin^2\theta),
\end{aligned} \tag{4}$$

where $\dot{\varepsilon}_{ij}$ denotes the strain rate component. The subscripts correspond to an x–y and 1–2 coordinate systems as shown in Fig. 3.

The relationship between fiber orientation angle and strain rate of each material principal direction under $\dot{\varepsilon} = 100\ \mathrm{s}^{-1}$ is shown in Fig. 12 for T7S-2. For the higher fiber-orientated specimens, it is clear that strain rate in the shear direction is much larger than those in longitudinal and transverse direction: $\dot{\gamma}_{12} = 428\ \mathrm{s}^{-1}$, $\dot{\varepsilon}_1 = 79.1\ \mathrm{s}^{-1}$ and $\dot{\varepsilon}_2 = -11.6\ \mathrm{s}^{-1}$ at 10° off-axis specimen. On the other hand, for the lower fiber-orientated specimens, strain rate in transverse directions becomes

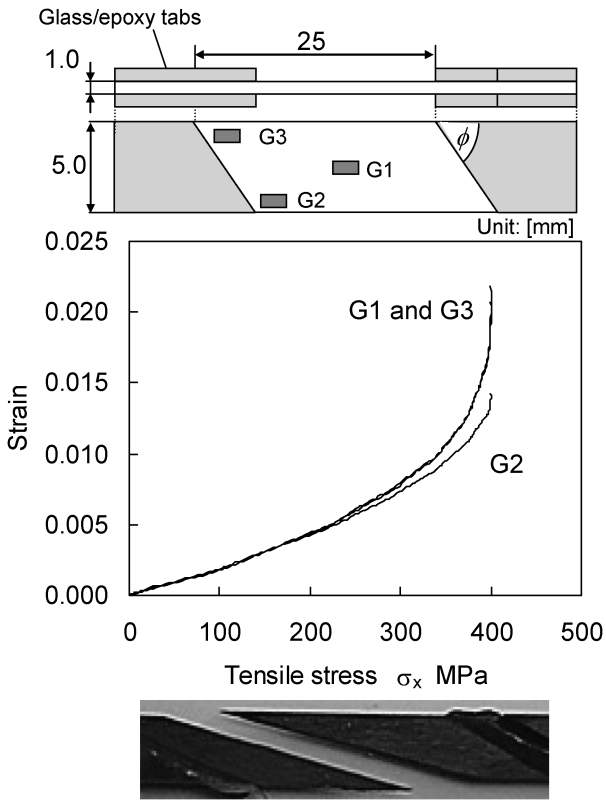

(b)

Figure 8. (Continued.)

dominant. According to the experimental results of 90° specimens in Table 2, the transverse strain rate effect on tensile strength is relatively small. This result implies that the shear strain rate has a great influence on the strain rate effect on tensile strength of carbon/epoxy composites.

4.2. Comparison of Fracture Behavior

To clarify the fracture behaviors of carbon/epoxy composites under dynamic loading, fracture surface observation was carried out by using a scanning electron microscope (SEM). The fracture surfaces for 10, 30 and 90° specimens of T7S-2 are shown in Fig. 13(a) at static and $\dot{\varepsilon} = 100\ \mathrm{s}^{-1}$ (dynamic) conditions. In the static test, it is clear that the crack propagates along the interface between the fiber and the matrix. On the other hand, in the dynamic test, the crack propagation area consists not only of the fiber/matrix interface but also of the matrix itself. Furthermore, the area ratio of matrix fracture in off-axis specimen strongly depends on the fiber orientation angle, i.e. the fracture surface of 10° off-axis specimens is dominated by the matrix failure, while the interfacial debonding is predominant in 90° specimens. The comparison of fracture surfaces for 10, 30 and 90° specimens of TR5S-m are

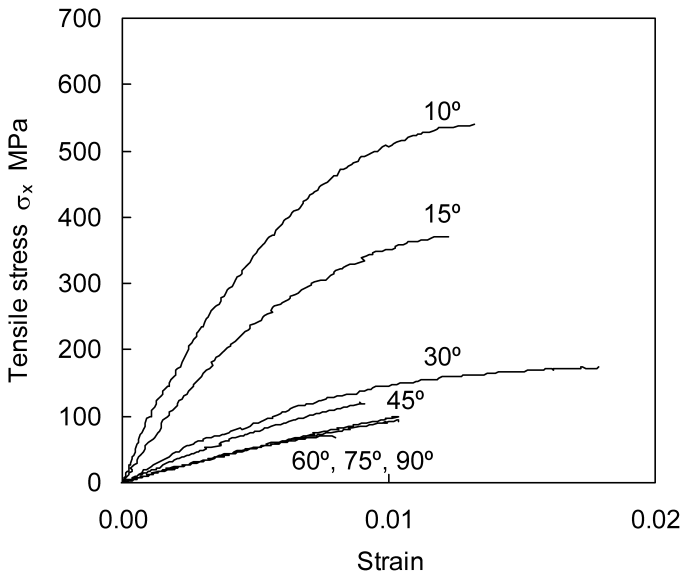

(a)

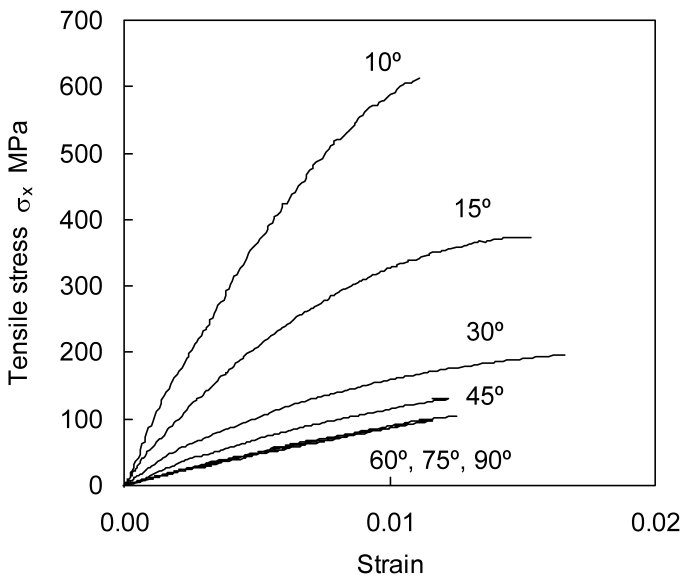

(b)

Figure 9. (a) Stress–strain curves for the 10, 15, 30, 45, 60, 75 and 90° specimens at a strain rate of 100 s^{-1}, T700S/2500 composite; (b) stress–strain curves for the 10, 15, 30, 45, 60, 75 and 90° specimens at a strain rate of 100 s^{-1}, TR50/modified epoxy composite.

shown in Fig. 13(b) at static and $\dot{\varepsilon} = 100\ s^{-1}$ (dynamic) conditions. No significant difference can be observed in the fracture surface between under static and dynamic conditions. The fracture behavior translation does not occur virtually in the TR5S-m system.

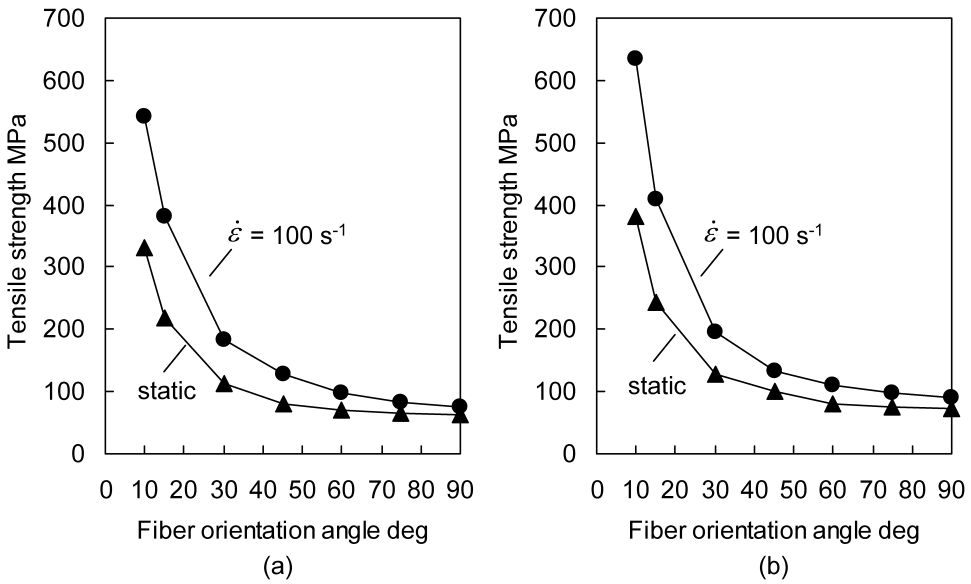

Figure 10. Comparison of tensile strength between static and strain rate of 100 s^{-1}.

Table 2.
A summary of tensile strength for stain rate of 100 s^{-1}

Fiber orientation angle	T700S/2500 (MPa)		TR50S/modified epoxy (MPa)	
	Static condition	Strain rate: 100 s^{-1}	Static condition	Strain rate: 100 s^{-1}
10°	330.4	541.3	382.3	635.5
15°	218.3	382.2	243.5	409.0
30°	113.4	183.5	127.0	194.9
45°	80.9	128.0	100.5	134.2
60°	70.3	98.0	79.6	109.6
75°	65.1	84.0	74.6	97.4
90°	63.1	74.4	72.6	91.6

By comparing the magnitude relation of fracture toughness between the fiber/matrix interface and matrix itself, the fracture behavior from static to dynamic conditions can be roughly explained. It has been reported that the fracture toughness of matrix decreases with the strain rate because of the embrittlement of epoxy resin [16]. Hence, if the decreasing ratio of matrix toughness is larger than that of the interface, the magnitude relation of fracture toughness will exchange at a specific strain rate. In other words, the crack propagates into the matrix itself when the fracture toughness of the matrix becomes lower than that of the fiber/matrix interface. In this study, this fracture behavior translation can be observed in T7S-2 system. It is obvious that this fracture translation produces the effect of matrix viscoelasticity more sensitively in relation to the tensile strength under high strain rate.

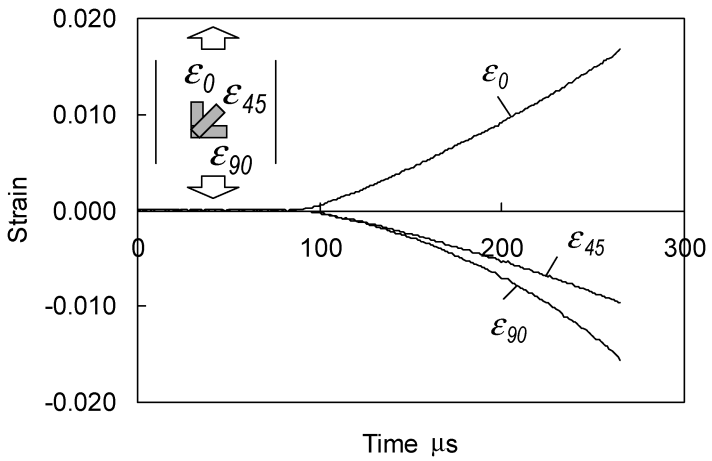

Figure 11. Typical examples of triaxial strain gauge outputs of 15° specimen (T700S/2500).

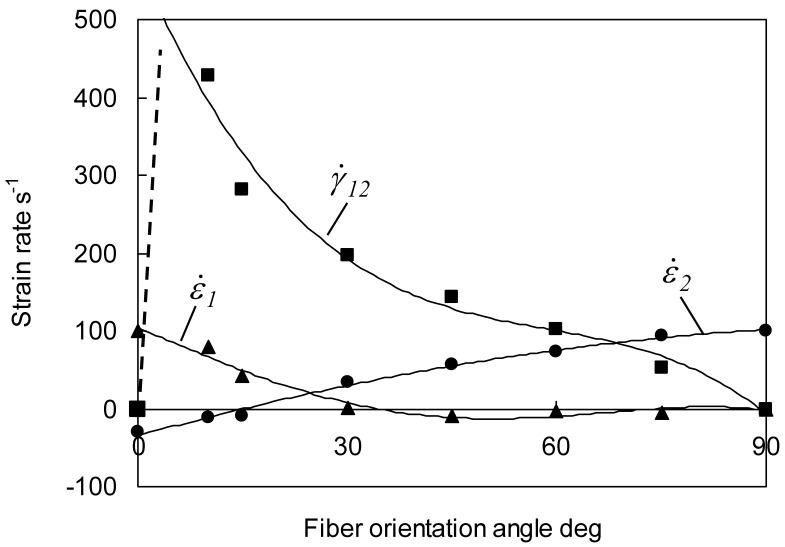

Figure 12. Comparisons of the strain rate in material principal direction at a strain rate of 100 s^{-1}.

These results imply that the magnitude relation of fracture toughness between the fiber/matrix interface and matrix itself is an important factor for characterizing the fracture behavior of carbon/epoxy composite under dynamic condition.

5. An Empirical Rate-Dependent Failure Criterion

A dual mode failure criterion, which is called as Hashin's failure criterion, is employed. This failure criterion is applied for prediction of the fiber breakage and matrix cracking. For the fiber breakage, it is defined as follows,

$$\sigma_1 \geqslant X, \tag{5}$$

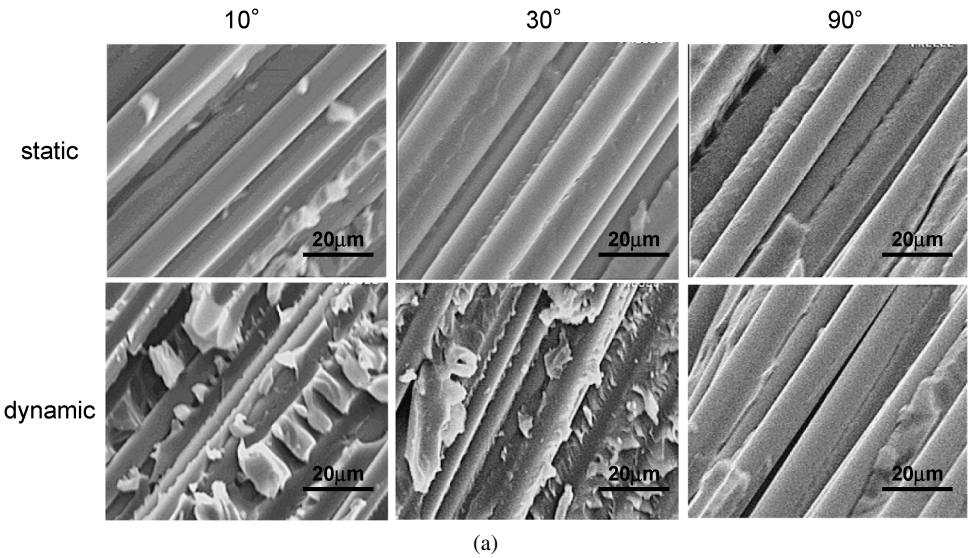

(a)

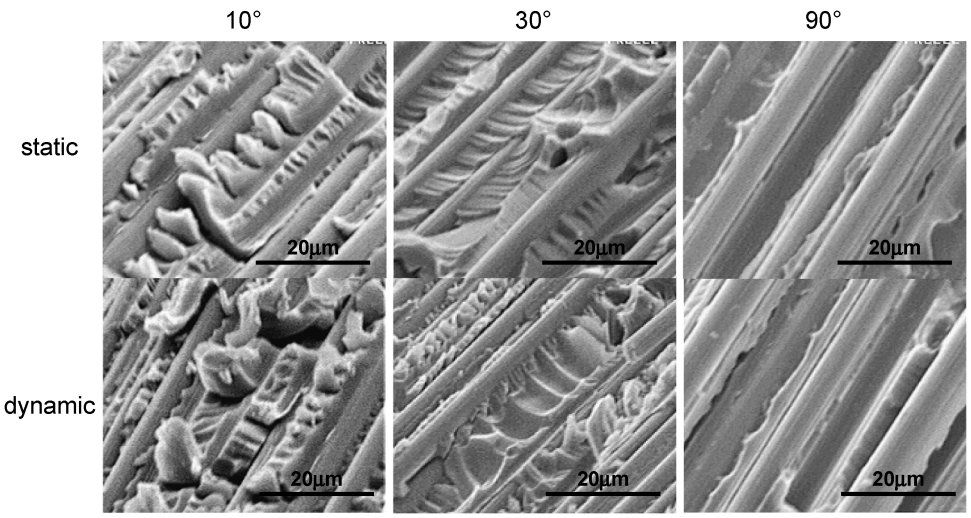

(b)

Figure 13. (a) Comparisons of fracture surface between static and dynamic conditions for 10, 30 and 90° specimens (T700S/2500); (b) comparisons of fracture surface between static and dynamic conditions for 10, 30 and 90° specimens (TR50S/modified epoxy).

where the stresses σ_{ij} refer to the principal material direction and X is the longitudinal strength. This equation is applicable for predicting the dynamic tensile strength of carbon/epoxy composite, since the experimental result shows that the X is independent of strain rate [9].

For the matrix or interfacial dominated failures, the failure criterion is given by

$$\frac{\sigma_2^2}{Y^2} + \frac{\tau_{12}^2}{S^2} = 1, \tag{6}$$

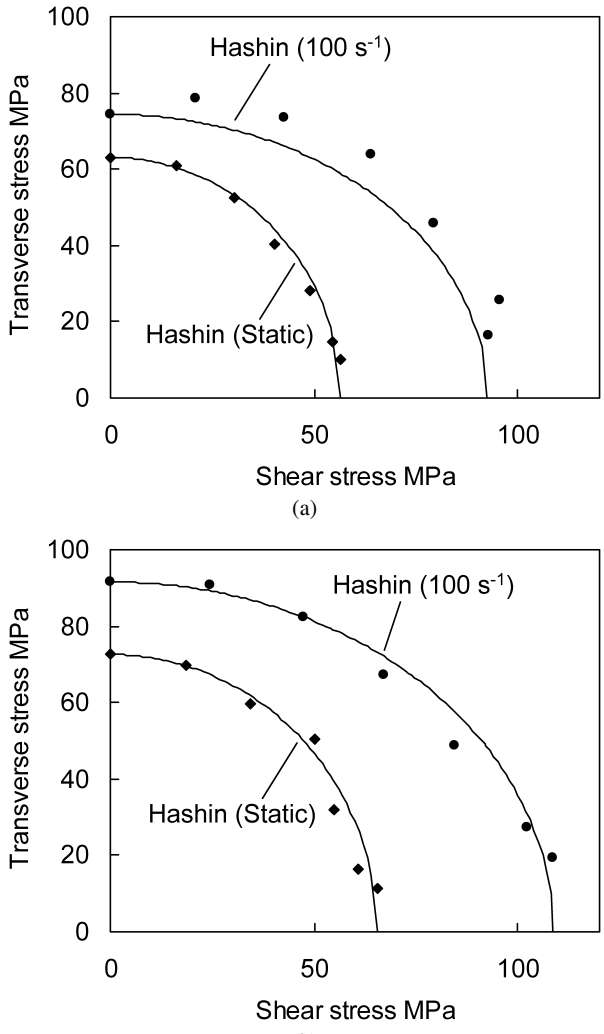

Figure 14. (a) Comparison of the experimental and predicted tensile strength (Hashin's failure criterion) at the static condition, and strain rate of 100 s^{-1} for off-axis specimens (T700S/2500); (b) comparison of the experimental and predicted tensile strength (Hashin's failure criterion) at the static condition, and strain rate of 100 s^{-1} for off-axis specimens (TR50S/modified epoxy).

where Y and S indicate the strength in transverse and shear direction for each strain rate, respectively. The results obtained from this criterion are plotted in Fig. 14(a) and 14(b) against the experimental data obtained at the static condition, and $\dot{\varepsilon} = 100\ s^{-1}$. In the failure envelope predictions, Y at $\dot{\varepsilon} = 100\ s^{-1}$ is derived from the experimental results of 90° and S at $\dot{\varepsilon} = 100\ s^{-1}$ is derived from that of 10° off-axis specimens with the transformation equations of stress. For TR5S-m composite, the tensile strength at both the strain rate conditions can be characterized quite well using the Hashin's failure criterion. Also, it characterizes well the

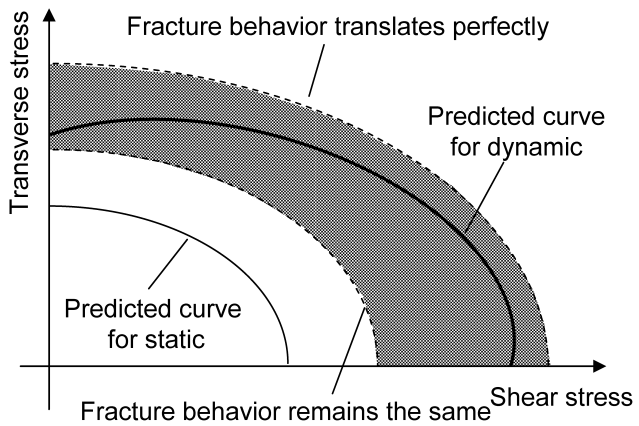

Figure 15. An illustration of basic concept for simple rate-dependent failure criterion.

tensile strength of T7S-2 at static condition. However, the model predictions of T7S-2 at $\dot{\varepsilon} = 100\ \mathrm{s}^{-1}$ are in poor agreement with the experiment. This disagreement is mainly caused by the fracture behavior translation from static to dynamic conditions. For accurate prediction of dynamic tensile strength of carbon/epoxy composites, this fracture behavior translation must be incorporated. However, it accommodates with difficulty the proposal to include the accurate rate-dependent failure criterion that involves the fracture behavior translation. In this study, an empirical rate-dependent failure criterion based on Hashin's failure criterion is proposed as follows:

$$\frac{\{\sigma_2 \cos(\varphi\dot{\varepsilon}) - \tau_{12} \sin(\varphi\dot{\varepsilon})\}^2}{Y^2} + \frac{\{-\sigma_2 \sin(\varphi\dot{\varepsilon}) + \tau_{12} \cos(\varphi\dot{\varepsilon})\}^2}{S^2} = 1, \qquad (7)$$

where the parameter φ corresponds to the fracture behavior translation and can be determined from the experimental results of the representative off-axis specimen. It is clear from equation (7) that this failure criterion indicates the geometry of a spheroid and φ is the angle of rotation. The basic concept of this criterion is illustrated in Fig. 15. The proposed failure criterion is represented to exist in the shaded area, which is surrounded by the two hypothetical curves (dashed line). The upper and lower curves indicate the hypothetical curve whose fracture behavior translates perfectly and remains the same, respectively.

Figure 16(a) and 16(b) shows the model prediction of tensile strength for T7S-2 and TR5S-m. In order to give an in-depth discussion, the model prediction of T7S-2 at $\dot{\varepsilon} = 50\ \mathrm{s}^{-1}$ is compared with the experimental results. Good agreement can be seen between experimental data and predicted curves even if strain rate changes. Further, it is also suggested that the parameter φ is related to the level of fracture behavior translation since φ obtained from T7S-2 is lager than that from TR5S-m.

As the proposed failure criterion is just an empirical formula, it is difficult to find out the physical implications of the parameter φ. Furthermore, the validity of this criterion has been just verified until the strain rate of $100\ \mathrm{s}^{-1}$. However, the model prediction can be calculated from the experimental result of 90° (transverse

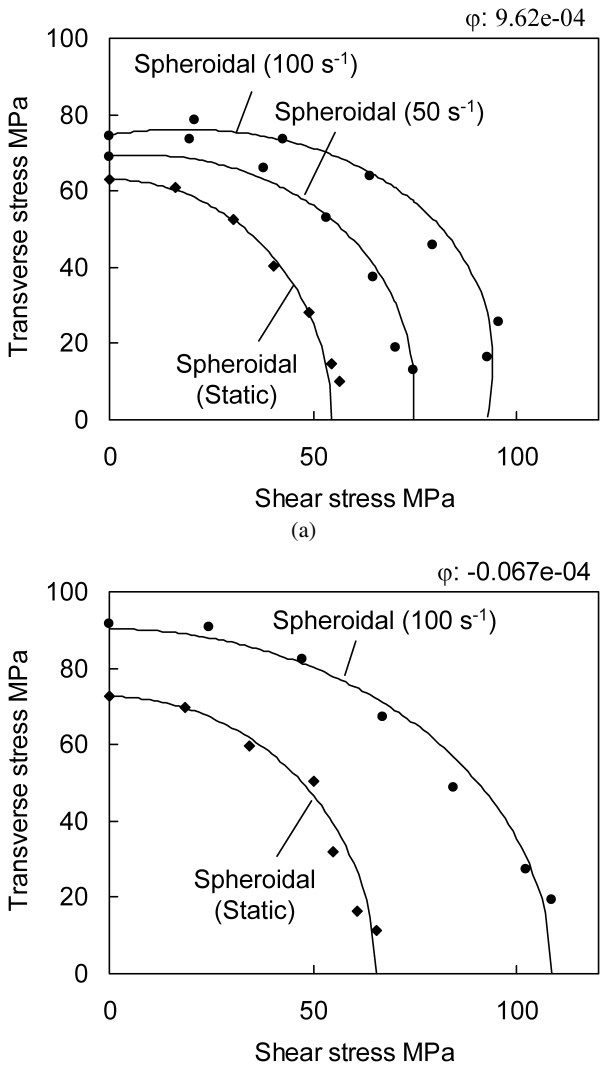

Figure 16. (a) Comparison of the experimental and predicted tensile strength (spheroidal failure criterion) at the static condition, strain rate of 50 s^{-1} and strain rate of 100 s^{-1} for off-axis specimens (T700S/2500); (b) comparison of the experimental and predicted tensile strength (spheroidal failure criterion) at the static condition, and strain rate of 100 s^{-1} for off-axis specimens (TR50S/modified epoxy).

strength), 10° (shear strength), and one typical off-axis specimens. Due to its simplicity, it is easy to incorporate into numerical software.

6. Conclusions

In this study, the tensile strength of unidirectional carbon/epoxy composites is characterized. Two different carbon/epoxy composite systems — a unidirectional

T700S/2500 and TR50S/modified-epoxy — are tested at both static and dynamic conditions. An oblique tab is found experimentally to be more appropriate for the measurement of the dynamic tensile property for off-axis specimens. Experimental results show that both tensile strengths increases with strain rate, while the fracture behaviors are quite different. Further, the higher fiber-orientated specimens produce the more significant contribution to the tensile strength. By the use of the rosette analysis and the strain transformation equations, it is experimentally found that the shear strain rate produces the more significant contribution to dynamic tensile strength. An empirical rate-dependent failure criterion, in which fracture behavior translation is incorporated, is proposed based on the Hashin's failure criterion. The model prediction agrees well with the experimental data of two carbon/epoxy composites until the strain rate of 100 s^{-1}. Although the proposed criterion is just an empirical formula, it is quite simple and easy to incorporate into numerical software.

Acknowledgements

We wish to thank Dr. Yoshizawa and Nippon Steel Composite Co. Ltd. for their generous support.

References

1. T. Nishiwaki, *SAMPE J.* **38**, 80–82 (2002).
2. Q. Bing and C. T. Sun, *Compos. Sci. Technol.* **65**, 2481–2491 (2005).
3. C. T. Sun and K. J. Yoon, *J. Compos. Mater.* **25**, 1297–1313 (1991).
4. C. A. Ross, W. H. Cook and L. L. Wilson, *Exper. Technol.* **November**, 30–33 (1984).
5. Z. G. Liu and C. Y. Chiem, *Exper. Technol.* **March**, 20–21 (1988).
6. S. V. Thiruppukuzhi and C. T. Sun, *Compos. Sci. Technol.* **61**, 1–12 (2001).
7. J. Harding and L. M. Welsh, *J. Mater. Sci.* **18**, 1810–1826 (1983).
8. G. H. Staab and A. Gilat, *J. Compos. Mater.* **29**, 1308–1320 (1995).
9. N. Taniguchi, T. Nishiwaki and H. Kawada, *Adv. Compos. Mater.* **16**, 167–180 (2007).
10. Z. Hashin, *J. Appl. Mech.* **47**, 329–334 (1980).
11. F. Pierron and A. Vautrin, *Compos. Sci. Technol.* **56**, 483–488 (1996).
12. C. T. Sun and I. Chung, *Composites* **24**, 619–623 (1993).
13. K. Ogawa, A. Kuraishi, T. Nishida and F. Sugiyama, *J. Soc. Mater. Sci., Japan* **45**, 799–804 (1996).
14. K. F. Graff, *Wave Motion in Elastic Solids*. Dover Publications, Inc., Mineola, NY (1991).
15. J. Tsai and C. T. Sun, *Intl. J. Solid Struct.* **41**, 3211–3224 (2004).
16. A. J. Kinloch and R. J. Young, *Fracture Behavior of Polymers*. Elsevier, The Netherlands (1983).